A Comparison of Lidar and Balloon-Borne Particle Counter Measurements of the Stratospheric Aerosol 1974–1980

T. J. SWISSLER, P. HAMILL AND M. OSBORN

Systems and Applied Sciences Corporation, Hampton, VA 23666

P. B. RUSSELL

SRI International, Menlo Park, CA 94025

M. P. MCCORMICK

NASA Langley Research Center, Hampton, VA 23665

(Manuscript received 4 May 1981, in final form 1 December 1981)

ABSTRACT

We compare a series of 85 dustsonde measurements and 84 lidar measurements made in midlatitude North America during 1974–80. This period includes two major volcanic increases (Fuego in 1974 and St. Helens in 1980), as well as an unusually clean, or background, period in 1978–79. An optical modeling technique is used to relate the dustsonde-number data to the lidar-backscatter data. The model includes a range of refractive indices and of size distribution functional forms, to show its sensitivity to these factors. Moreover, two parameters of each size distribution function are adjustable, so that each distribution can be matched to any two-channel dustsonde measurement.

We show how the mean particle radius for backscatter, r_B, changes in response to size distribution changes revealed by the dustsonde channel ratio, $N_{r>0.15}/N_{r>0.25}$. ($N_{r>x}$ is the number of particles with radius larger than x microns.) In early 1975, just after the Fuego injection, $N_{r>0.15}/N_{r>0.25}$ was ~3, and the corresponding r_B was ~0.5 μm; by early 1980, when $N_{r>0.15}/N_{r>0.25}$ had increased to eight or larger, r_B had correspondingly decreased to ~0.25 μm. Throughout the 1975–76 Fuego decay, r_B always exceeded 0.3 μm; thus, lidar backscatter was influenced primarily by particles larger than those that contribute most to $N_{r>0.15}$ and $N_{r>0.25}$. This is in accord with the shorter lidar background-corrected, $1/e$ decay time: 7.4 months, versus 10.4 and 7.9 months for $N_{r>0.15}$ and $N_{r>0.25}$.

The modeling technique is used to derive a time series of dustsonde-inferred peak backscatter mixing ratio, which agrees very well with the lidar-measured series. The best overall agreement for 1974–80 is achieved with a mixture of refractive indices corresponding to aqueous sulfuric acid at about 210 K with an acid-weight fraction between 0.6 and 0.85.

1. Introduction

Experimental observations of the stratospheric aerosol layer have been made for more than 40 years with a variety of different *in situ* and remote sensors. Junge *et al.* (1961) employed particle impactors flown on balloons to make *in situ* measurements of the stratospheric sulfate aerosol layer. Balloon-borne light-scattering particle counters called dustsondes have been used extensively by researchers at the University of Wyoming for a number of years (Rosen, 1964, 1971; Hofmann *et al.*, 1975; Pinnick *et al.*, 1976; Hofmann and Rosen, 1981). Ground-based lidar systems to make remote measurements of the stratospheric aerosol have been developed by a number of different groups (Fiocco and Grams, 1964; Collis and Ligda, 1966; Russell *et al.*, 1976; Russell and Hake, 1977; McCormick *et al.*, 1978). Airborne lidar systems have also been developed to study the stratospheric aerosol (Fox *et al.*, 1973; Fernald and Schuster, 1977; Russell *et al.*, 1981b). More recently, satellite-borne radiometers [SAM II(Stratospheric Aerosol Measurement) and SAGE (Stratospheric Aerosol and Gas Experiment)] have been developed (McCormick *et al.*, 1979) to monitor and map out the global distribution of stratospheric aerosols.

Comparisons between different aerosol measuring systems have been previously reported for single field experiments. For example, Northam *et al.* (1974) compared dustsonde and lidar measurements and Russell *et al.* (1976) compared lidar measurements with filter-collected samples. An extensive series of comparative experiments designed to provide correlative measurements for the SAM II and SAGE projects were recently carried out, and results from the comparison of stratospheric aerosol measurements made by lidar, dustsonde, and the SAM II satellite system have been reported (Russell *et al.*, 1981b).

In this paper we present a comparison between a

0022-4928/82/040909-08$06.00

long series of stratospheric lidar measurements and a series of dustsonde measurements made during the same time frame but at different geographic locations.

The lidar measurements are those which have been obtained routinely at Hampton, Virginia (37.1°N, 76.3°W) by the Langley Research Center's 48-inch lidar-system since 1974. The dustsonde measurements are those made monthly by the University of Wyoming at Laramie (41.2°N, 105°W). The extensive data sets acquired with these two instruments during the time period 1974–80 permit a long-term comparison of the two different measurement techniques. The 1974–80 interval is especially interesting for comparison because it includes a variety of aerosol conditions. Specifically, this period includes background stratospheric aerosol concentrations previous to the eruption of Volcán de Fuego in Guatemala in late 1974, followed by volcanically influenced concentrations for several years, followed by a return to background conditions in 1978–79. Recent eruptions of other volcanoes, such as La Soufrière (St. Vincent, 13.3°N, 61.2°W, April 1979) and Sierra Negra (Galapagos Island, 0.8°S, 91.2°W, November 1979) did not as significantly influence the data in the mid-latitude stratospheric aerosol peak (~20 km altitude) before 1980 (Rosen and Hofmann, 1980). However, the effect of Mt. St. Helens (Washington State, 42.2°N, 122.2°W, May 1980) was quite large. This is due, in part, to the fact that the measurements were made at latitudes close to that of Mt. St. Helens and therefore the volcanic plume did not have time to disperse before the measurements were made.

In order to carry out the comparison between the dustsonde results and the lidar measurements, it was necessary to convert the dustsonde-measured particle number concentrations to equivalent aerosol backscatter mixing ratios. This conversion requires information on the size distribution, refractive index, and shape of the aerosol particles. Since detailed information on these properties was not available for most of the dustsonde or lidar measurements, we have used the aerosol optical model described in Russell *et al.* (1981a) to supply this information. Because previous measurements and the concurrent dustsonde data do not totally constrain this model, it retains a certain allowed range for its parameters. Thus, the goodness of fit between lidar-measured and dustsonde-plus-model-inferred backscatter in the present comparison can shed some light on the most probable values of these parameters within their remaining range of freedom.

2. Instrumentation

The balloon-borne dustsonde pumps ambient air in a well-defined stream through an illuminated chamber where individual aerosol particles scatter light into photodetectors. The output from these detectors undergoes pulse height discrimination such that the integral concentration of aerosol particles with radii greater than 0.15 μm (channel I) and greater than 0.25 μm (channel II) can be determined. For a detailed description of the instrument and the method of calibration, see Hofmann *et al.* (1975).

The lidar system used in these studies has a 1–2J ruby laser ($\lambda = 0.6943$ μm) with a 48-inch (1.22 m) Cassegrainian configured telescope mounted on a mobile platform to collect the backscattered laser light. The backscattered signal is analyzed together with rawinsonde-derived molecular density data to infer profiles of the aerosol backscatter mixing ratio. The rawinsonde data were obtained from Wallops Island, Virginia (120 km northeast of the lidar system). For details of the instrument and analysis procedures see McCormick *et al.* (1978) and Russell *et al.* (1979).

3. Data

The time series of stratospheric peak aerosol mixing ratio for the two-channel dustsonde measurements and the lidar measurements are shown in Fig. 1. The dustsonde data represent 85 soundings made over a period of 79 months (Hofmann and Rosen, 1980 and 1981). Similarly, the lidar data, representing 84 measurements made over a period of 82 months, are plotted below the dustsonde data. For each sensor the value of peak ratio shown for each date was obtained by averaging all of the measured ratios obtained within ±0.5 km of the maximum stratospheric value (which was generally near 20 km altitude). The intense narrow dust layers observed by the lidar system immediately following the eruption of Mt. St. Helens were averaged over a vertical scale of ±0.15 km.

The notable features of Fig. 1 are the rapid increase and subsequent decay in the peak aerosol mixing ratio between late 1974 and 1979, and the appearance of a second peak in 1980. These are due to the volcanic eruptions of Volcán de Fuego (1974) and Mt. St. Helens (1980). The Fuego eruptions (Guatemala, 14.5°N, 91°W), which took place in October 1974, injected a large amount of particulate matter into the stratosphere, as did the Mt. St. Helens eruptions in May 1980. Mt. St. Helens is also reported to have injected large amounts of sulfurous gases into the stratosphere. The record also shows several minor increases in aerosol loading which could be due to other volcanic eruptions but which might simply be indicative of other natural variations in the layer.

We have calculated decay times for the Fuego volcanic component in Fig. 1 by first subtracting-off the background (1978–79) values (6 and 1.1 particles mg^{-1} for $r \geq 0.15$ and $r \geq 0.25$ μm, respectively, and

0.07 for backscatter mixing ratio), and then fitting exponential curves to the resulting data for the period January 1975–April 1977 (see also Hofmann and Rosen, 1981). The resulting $(1/e)$ decay times are 10.4, 7.9 and 7.4 months for dustsonde channels I and II and the lidar, respectively. It is interesting to consider the reasons for these different decay times. Since channel II measures the number density of larger particles, it is not surprising that it should show a smaller decay time than channel I, for the larger particles will have a greater fall velocity and sedimentation will be faster. Since the size distributions are steep, the measured values in each channel are most strongly influenced by particles with radius nearly equal to the lower cut off. The $(1/e)$ decay time for the lidar backscatter ratio is shorter than either of the dustsonde channel decay times. This suggests that the lidar measurement is sensitive to even larger particle sizes; however, it should be noted that this is an integral optical measurement and depends not only on size distribution but also on scattering properties of the aerosol such as the refractive index and particle shape, parameters which could be changing with time.

4. Lidar data analysis

The aerosol backscatter coefficient can be described by

$$B_A(\lambda, Z) = \int \sigma_B(r, \lambda, m) n(r, Z) dr, \qquad (1)$$

where $\sigma_B(r, \lambda, m)$ is the backscatter cross-section at wavelength λ, particle radius r, and refractive index m; $n(r, Z)$ is the particle number density (per unit volume and unit radius interval) at altitude Z. The lidar backscatter mixing ratio is then simply defined as

$$b(\lambda, Z) = B_A(\lambda, Z)/B_M(\lambda, Z), \qquad (2)$$

where $B_M(\lambda, Z)$ is the gaseous backscattering function as derived from the simultaneous rawinsonde data. A measure of the size of the particles that contribute most to the integrated backscatter in (1) can be obtained by defining a mean or effective radius for backscattering as (e.g., Hansen and Travis, 1974)

$$r_B(\lambda, m) = \frac{\int r \sigma_B(r, \lambda, m) n(r) dr}{\int \sigma_B(r, \lambda, m) n(r) dr}. \qquad (3)$$

As indicated by Pinnick *et al.* (1976), at least three different types of size distribution (lognormal, exponential, and power law) are consistent with dustsonde measurements of the stratospheric aerosol. Moreover, other types of size distributions (zold, modified gamma) have also been recommended as discussed in Russell *et al.* (1981a).

Besides the size distribution, one must also make an assumption on the composition of the aerosol particles in order to carry out a comparison between the lidar and dustsonde measurements. There is a large body of experimental and theoretical evidence indicating that the stratospheric aerosol particles are liquid spheres of aqueous sulfuric acid with an acid/water mass ratio between 60/40 and 85/15 with a value of about 75/25 being most likely (Rosen, 1971; Toon and Pollack, 1973; Russell and Hake, 1977; Rosen *et al.*, 1978; Hamill *et al.*, 1979; Toon *et al.*, 1979; Turco *et al.*, 1979). Refractive index values of $1.40 - 0i$, $1.42 - 0i$ and $1.43 - 0i$ span this range of sulfuric acid/water solution mixtures.

These refractive index values apply to temperatures near 300 K because this is where virtually all reported values were measured and, as a consequence, published stratospheric aerosol models to date have used these values (e.g., Pinnick *et al.*, 1976, Toon and Pollack, 1976); however, stratospheric temperatures are considerably smaller ($T \sim 190$–240 K). The temperature dependence of refractive index can be accounted for by using the Lorentz-Lorenz equation (Steele and Hamill, 1981). Pinkley

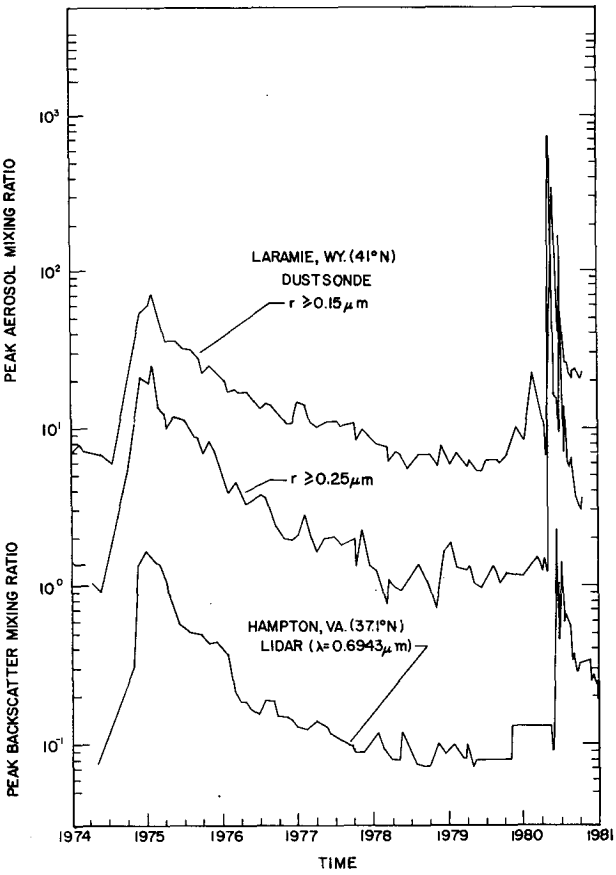

FIG. 1. Time sequence of peak aerosol mixing ratio from the two dustsonde channels and peak backscatter mixing ratio from the 48-inch lidar during 1974–80.

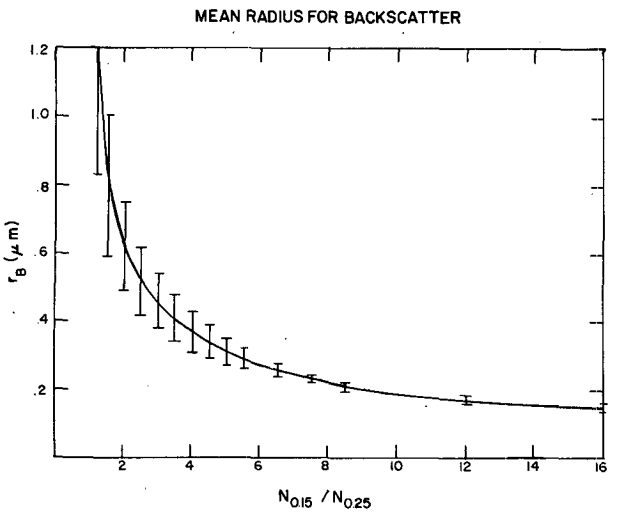

FIG. 2. Calculated mean radius for backscatter (r_B) as a function of channel ratio ($N_{0.15}/N_{0.25}$) evaluated using nine different size distribution functional forms and four indices of refraction ($m = 1.43 - 0i$; $m = 1.44 - 0i$; $m = 1.45 - 0i$; $m = 1.46 - 0i$). The vertical bars represent ± one standard deviation from the mean due to different assumptions made in the calculations.

and Williams (1976) have measured near-infrared optical constants of sulfuric acid at 250 K and found that the Lorentz-Lorenz temperature correction of the refractive index works quite well. At stratospheric temperatures (≈190–240 K), the refractive index of sulfuric acid/water solutions with mass fractions between 60/40 and 85/15 ranges from 1.43 − 0*i* to 1.46 − 0*i* for the wavelength 0.69 μm, or significantly larger than the 300 K values.

Assuming a size distribution and an index of refraction, Mie scattering theory can be used to calculate values for the mean radius for backscatter. We have carried out this analysis using the nine size-distribution types listed in Russell *et al.* (1981a) and the range of values of particle composition mentioned above. The free parameters in the size distributions were varied in such a way that the ratio $N_{r>0.15}/N_{r>0.25}$ (the dustsonde "channel ratio") ranged from 1.2 to 16. In Fig. 2 we present the results of these calculations as a plot of mean backscatter radius versus channel ratio for lidar light of wavelength 0.6943 μm and for the cold temperature mix of sulfuric acid refractive indices. The vertical bars represent the $\pm 1\sigma$ range of values obtained when different size distribution types and different particle compositions were assumed. Although it is clear that the backscatter radius is somewhat sensitive to the assumptions on size distribution and composition, the figure shows a definite trend in backscatter radius as a function of channel ratio. The mean radius for backscatter approaches a minimum value of ~0.15 μm as the dustsonde channel ratio gets large.

In Fig. 3a we plot the history of the measured dustsonde channel ratio over the 1974–80 time period. Fig. 3b shows the corresponding history of the mean backscatter radius as derived from the channel ratios in Fig. 3a and the results of Fig. 2. This history indicates that during background periods, for example after the spring of 1977, the ruby-lidar backscatter was influenced primarily by aerosol particles of radii <0.30 μm. However, during the period January 1975–January 1977 (post-volcanic aerosol), the mean backscatter radius was between 0.30 and 0.50 μm. Thus the fact that the backscatter mixing ratios decayed faster than particle number both in dustsonde channel I and in channel II is consistent with the indication of Fig. 3b that larger particle sizes most strongly influenced ruby lidar backscatter in the immediate post-volcanic period.

5. Conversion of dustsonde particle number to backscatter

Employing the same principle composition assumptions as described above and the stratospheric aerosol size distributions given in Russell *et al.*, 1981a, we have calculated the mean or expected conversion factor from aerosol backscatter to channel I particle count as a function of the measured dustsonde channel ratio $N_{0.15}/N_{0.25}$. These results are

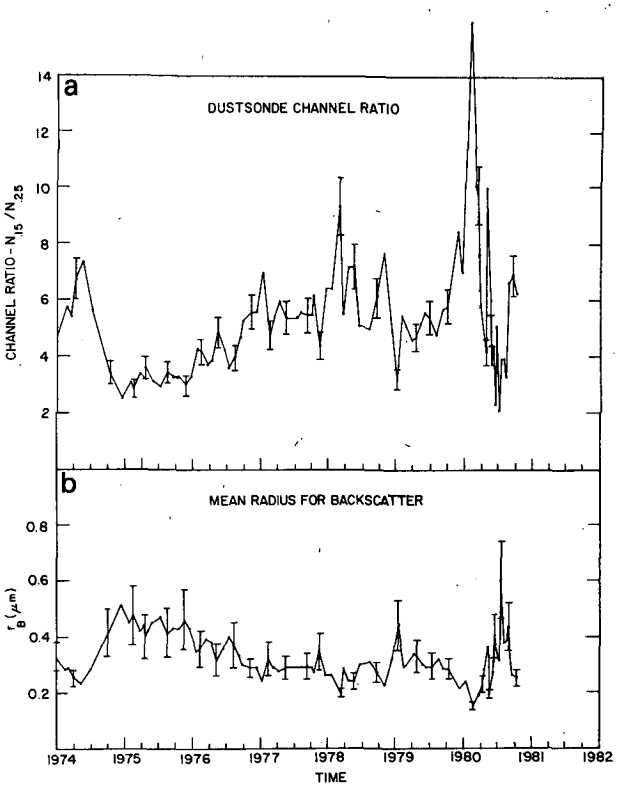

FIG. 3. (a) Time history of dustsonde channel ratio over time period 1974–80. (b) Time history of mean radius for backscatter over time period 1974–80 as derived from channel ratio of (a) and results of Fig. 2.

plotted in Fig. 4 where we give the mean (and standard deviation) obtained for the set of nine size-distribution-function types and the mix of values for the refractive index ($1.43 - 0i$, $1.44 - 0i$, $1.45 - 0i$ and $1.46 - 0i$).

The results of Fig. 4 were obtained in the following manner. First, the free parameter of each model size distribution type was varied to yield a particular $N_{r>0.15}/N_{r>0.25}$ value (e.g., $N_{r>0.15}/N_{r>0.25} = 4.0$). Then, selecting an index of refraction appropriate for the assumed composition of the aerosol particles, the backscatter coefficient for light of wavelength 0.6943 μm was calculated utilizing Eq. (1) and a Mie scattering code. The results of this analysis were used to obtain, for each model size distribution type, the ratio of backscatter to number of particles with radii >0.15 μm. Averaging the values obtained for the nine different size distribution types then produced a single data point and error bar (standard deviation) on one of the curves of Fig. 4. Repeating this process for different values of $N_{r>0.15}/N_{r>0.25}$ and different refractive indices produced the curve of Fig. 4.

We have used the conversion-ratio results in Fig. 4 to derive expected backscatter mixing ratios from the dustsonde data in Fig. 1. In this analysis, we first assign the symbol ω to the model backscatter-to-number ratio, and the symbol $n_{r>0.15}$ to the Channel I number mixing ratio. Thus,

$$\omega \equiv B_A\,(0.69\ \mu\text{m})/N_{r>0.15}\,, \tag{4}$$

$$n_{r>0.15} \equiv N_{r>0.15}/\rho, \tag{5}$$

where ρ is the mass density of gaseous air at the height of interest. Combining (2), (4), and (5) yields

$$b\,(0.69\ \mu\text{m}) = \frac{\omega N_{r>0.15}}{B_M\,(0.69\ \mu\text{m})} = \frac{\omega n_{r>0.15}\rho}{B_M\,(0.69\ \mu\text{m})}, \tag{6}$$

$$b\,(0.69\ \mu\text{m}) = c n_{r>0.15}\,, \tag{7}$$

where

$$c \equiv \frac{\omega}{B_M\,(0.69\ \mu\text{m})/\rho}. \tag{8}$$

B_M is directly proportional to ρ and the denominator of (8) is given by

$$B_M\,(0.69\ \mu\text{m})/\rho = 4.54 \times 10^{-13}\ \text{m}^2\ \text{sr}^{-1}\ \text{mg}^{-1}. \tag{9}$$

The results of Fig. 4 can be combined with (7)–(9) in the following manner to derive expected backscatter mixing ratios from the dustsonde data in Figs. 1 and 3a. For any given dustsonde measurement of $N_{r>0.15}/N_{r>0.25}$ (Fig. 3a), the corresponding value of ω [i.e., $B_A\,(0.69\ \mu\text{m})/N_{r>0.15}$] is found from Fig. 4. This value of ω and the dustsonde-measured value of $n_{r>0.15}$ (Fig. 1) are then substituted into (7) to yield the corresponding dustsonde-inferred value for b (0.69 μm). The results, for the sulfuric-acid values of ω (Fig. 4), are shown by the dashed line in Fig. 5. These dustsonde-inferred values can be compared to the lidar-measured values indicated by the solid curve.

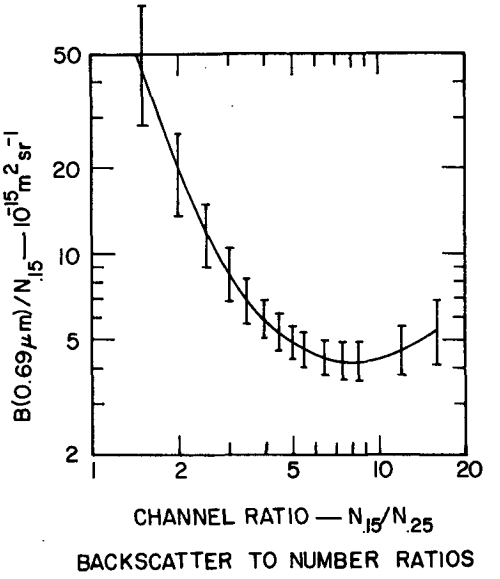

FIG. 4. Ratio of backscatter to number of particles with radius > 0.15 μm [$B(\lambda)/N_{0.15}$] as a function of channel ratio for different indices of refraction: a mix of values for sulfuric acid ($1.43 - 0i$, $1.44 - 0i$, $1.45 - 0i$ and $1.46 - 0i$) for $\lambda = 0.69$ μm. The curve represents the average obtained using nine different size distribution function types. Vertical bars represent ± one standard deviation of results for the nine different distribution types.

The overall agreement between the dustsonde-inferred and lidar-measured time series in Fig. 5 is quite good. Differences between the lidar-measured and dustsonde-inferred values on any given date range from 10 to 40%. However, this type of short term disagreement is to be expected given the differences in measurement place and time and the unknown details of size distribution and composition. The important point here is that, when averaged over several months, the lidar and dustsonde curves show excellent agreement from late 1974 to 1980. Consistent differences between the two measurements can be used to estimate possible changes in the optical properties of the aerosol particles.

6. Discussion

The results presented above show that average backscatter-to-number ratios obtained from nine different size distribution function types and several different but realistic values of index of refraction can be used to convert dustsonde measurements to backscatter profiles (and vice-versa) with considerable success. In Fig. 6 we plot *measured* values of $B_A\,(0.69\ \mu\text{m})/N_{r>0.15}$ as a function of channel ratio. That is, for a given date, we take the measured peak value of lidar backscatter coefficient and divide it by the measured peak number density determined by

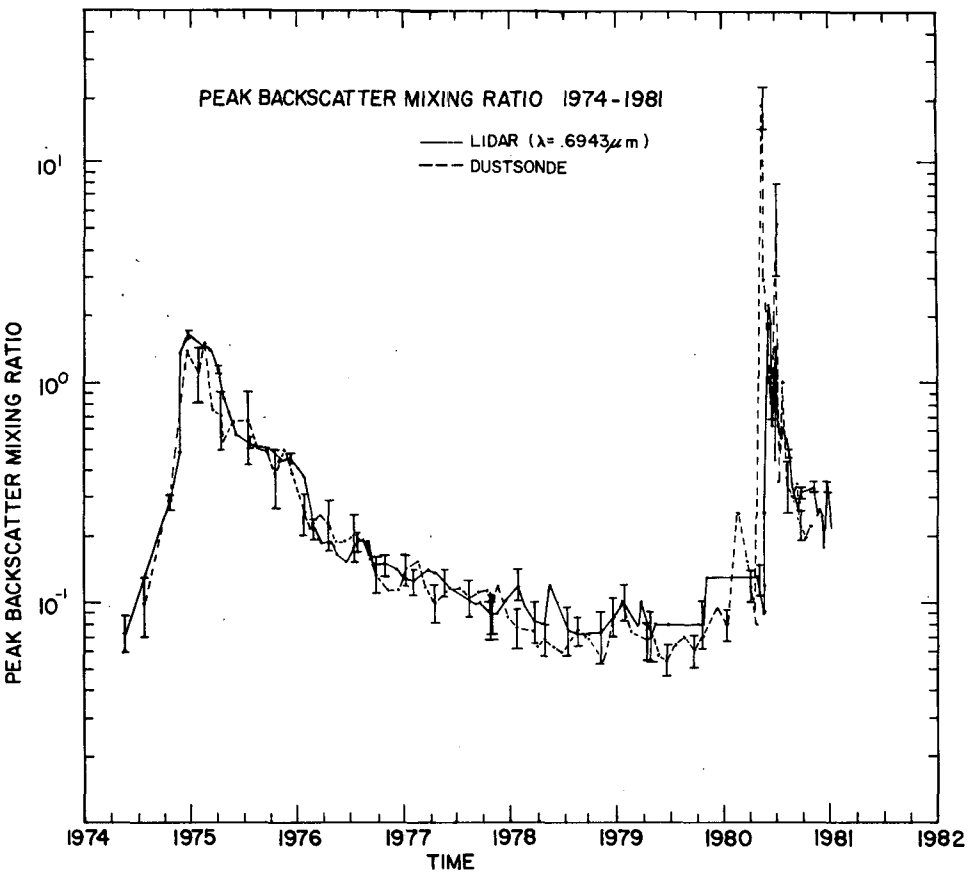

FIG. 5. Time history of lidar-measured and dustsonde-inferred peak backscatter mixing ratio during 1974–80. Dustsonde values were obtained using the sulfuric acid model conversion curve in Fig. 4. Lidar error bars are from the error analysis method of Russell *et al.* (1979). Dustsonde error bars include both dustsonde measurement uncertainty and the conversion uncertainties indicated by the error bars in Fig. 4.

dustsonde channel I. The resultant value is then plotted as a function of measured channel ratio. The curves on the figure represent the values predicted for some of the different refractive indices we have considered. The error bars on the cold refractive index curve for sulfuric acid ($1.43 - 0i$, $1.44 - 0i$, $1.45 - 0i$ and $1.46 - 0i$) represent the one sigma model uncertainty obtained when the different size distribution types and the range of refractive indices were assumed. The point labeled A indicates the typical measurement uncertainty in forming the ratio of measured lidar backscatter to peak channel I number density. It is interesting to note that some of the data points show a tendency toward the higher curves on the plot possibly indicating that there is a change in the aerosol model with time. Note, however, that the change in the channel ratio with time is accounted for in this plot since we are using $N_{0.15}/N_{0.25}$ as the independent variable.

The effect of including in the model a small imaginary component to the index of refraction ($0.005i$) has also been calculated. The result is to decrease the calculated B (0.69 μm) to $N_{0.15}$ ratio, thus lowering the model curves in Fig. 6 below the range of measured data points. Also in Fig. 5, the effect is to lower the dustsonde-derived backscatter results (dashed line) below the measured lidar results. Thus the evidence here indicates that the possibility of a small imaginary part to the index of refraction is not supported by these measurements, if one assumes that the particles are homogeneous spheres. Consideration of the effects of absorbing inhomogeneities within the particles is beyond the scope of this paper, but could possibly be attacked using the methods of Ackerman and Toon (1981).

Clearly, if model size distribution types are limited to the nine listed in Russell *et al.* (1981a), no single refractive index fits all of the data. However, an index of refraction mix is perhaps the best choice for most of the data. The middle curve of Fig. 6, the one for the cold refractive index values for sulfuric acid, best represents the collection of measured data points and involves the fewest assumptions on particle composition. It is also consistent with recent evidence ob-

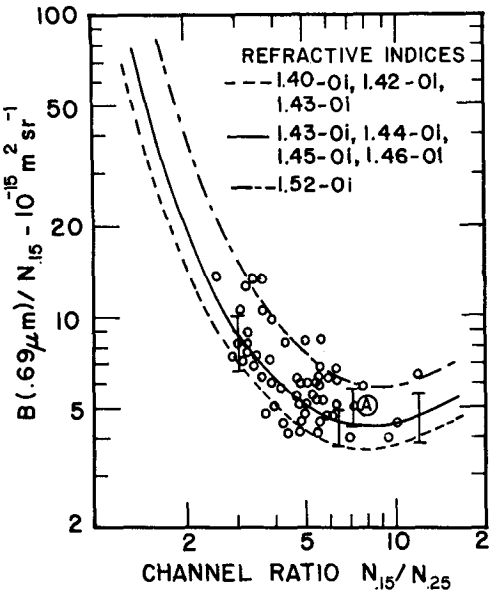

FIG. 6. Ratio of measured values of peak backscatter [B (0.69)] to measured dustsonde channel I peak value ($N_{0.15}$) plotted as function of channel ratio ($N_{0.15}/N_{0.25}$). The curves represent values predicted by using different indices of refraction.

tained by N. Farlow and co-workers (reported in Hayes *et al.*, 1980) indicating that there is no crystalline ammonium sulfate in samples of stratospheric particles when they are preserved in an inert atmosphere and analyzed under clean laboratory conditions. This does not mean that dissolved ammonium sulfate may not be in the particles or that crystalline ammonium sulfate may not exist in the aerosol at stratospheric temperatures; nevertheless, it does indicate that one should be quite careful before ascribing characteristics of the stratospheric particles to the presence of ammonium sulfate.

7. Conclusion

We have shown that it is possible to successfully compare a seven-year record of dustsonde and lidar measurements obtained at similar latitudes (41 and 37°N) but widely separated longitudes (105 and 76°W) by using optical modeling techniques. These techniques make use of the limited information on particle size distribution supplied by the dustsonde data themselves, but they fill in unmeasured size distribution details using a set of size distribution functions based on more detailed previous measurements and models. Similarly, the model uses a range of refractive indices that are consistent with previous composition measurements. The results given here show that lidar measurements, dustsonde measurements, and realistic optical models together give a very consistent picture of stratospheric aerosol behavior in 1974–80, including its response to two major volcanic injections.

Acknowledgments. We are grateful to James Rosen and David Hofmann for supplying dustsonde data and for helpful discussions. We are indebted to David Colburn for bringing to our attention the Lorentz-Lorenz method of accounting for refractive index–temperature dependence. This research was supported by the National Aeronautics and Space Administration through contracts NASI-14314 and NASI-15077.

REFERENCES

Ackerman, T. P., and O. B. Toon, 1981: Absorption of visible radiation in atmosphere containing mixtures of absorbing and nonabsorbing particles. *Appl. Opt.*, **20**, 3661–3667.

Collis, R. T. H., and M. G. H. Ligda, 1966: Note on lidar observations of particulate matter in the stratosphere. *J. Atmos. Sci.*, **23**, 255–257.

Fernald, F. G., and B. H. Schuster, 1977: Wintertime 1973 airborne lidar measurements of stratospheric aerosols. *J. Geophys. Res.*, **82**, 433–437.

Fiocco, G., and G. Grams, 1964: Observation of aerosol layer of 20 km by optical radar. *J. Atmos. Sci.*, **21**, 323–324.

Fox, R. J., G. W. Grams, B. G. Schuster and J. A. Weinman, 1973: Measurements of stratospheric aerosols by airborne laser radar. *J. Geophys. Res.*, **78**, 7789–7801.

Hamill, P., T. J. Swissler, R. P. Turco and O. B. Toon, 1979: Simulated lidar return from a one-dimensional stratospheric aerosol model. *Nature*, **278**, 149–152.

Hansen, J. E., and L. D. Travis, 1975: Light scattering in planetary atmospheres. *Space Sci. Rev.*, **16**, 527–610.

Hayes, D., K. Snetzinger, G. Ferry, V. Oberdeck and N. Farlow, 1980: Reactivity of stratospheric aerosols to small amounts of ammonia in the laboratory environment. *Geophys. Res. Lett.*, **1**, 974–976.

Hofmann, D. J., and J. M. Rosen, 1980: Stratospheric sulfuric acid layer: Evidence for an anthropogenic component. *Science*, **208**, 1368–1370.

——, and ——, 1981: On the background stratospheric aerosol layer. *J. Atmos. Sci.*, **38**, 168–181.

——, ——, T. J. Pepin and R. G. Pinnick, 1975: Stratospheric aerosol measurements I. Time variations at northern mid-latitudes. *J. Atmos. Sci.*, **32**, 1446–1456.

Junge, C. E., C. W. Chagon and J. E. Manson, 1961: Stratospheric aerosols. *J. Meteor.*, **18**, 81–108.

McCormick, M. P., T. J. Swissler, W. P. Chu and W. H. Fuller, Jr., 1978: Post-volcanic stratospheric aerosol decay as measured by lidar. *J. Atmos. Sci.*, **35**, 1296–1303.

——, P. Hamill, T. J. Pepin, W. P. Chu, T. J. Swissler and L. R. McMaster, 1979: Satellite studies of the stratospheric aerosol. *Bull. Amer. Meteor. Soc.*, **60**, 1038–1046.

Northam, G. B., J. M. Rosen, S. H. Melfi, T. J. Pepin, M. P. McCormick, D. J. Hofmann and W. H. Fuller, Jr., 1974: A comparison of dustsonde and lidar measurements of stratospheric aerosols. *Appl. Opt.*, **13**, 2416–2421.

Pinkley, L. W., and D. Williams, 1976: The infrared optical constants of sulfuric acid at 250°K. *J. Opt. Soc. Amer.*, **66**, 122–124.

Pinnick, R. G., J. M. Rosen and D. J. Hofmann, 1976: Stratospheric aerosol measurements III: Optical model calculations. *J. Atmos. Sci.*, **33**, 304–315.

Rosen, J. M., 1964: The vertical distribution of dust to 30 kilometers. *J. Geophys. Res.*, **64**, 4673–4676.

——, 1971: The boiling point of stratospheric aerosols. *J. Appl. Meteor.*, **10**, 1044–1045.

——, and D. J. Hofmann, 1980: A stratospheric aerosol increase. *Geophys. Res. Lett.*, **7**, 669–672.

——, —— and S. P. Singh, 1978: A steady-state stratospheric aerosol model. *J. Atmos. Sci.*, **35**, 1304–1313.

Russell, P. B., and R. D. Hake, 1977: The post-Fuego stratospheric aerosol: Lidar measurements with radiative and thermal implications. *J. Atmos. Sci.*, **34,** 163–177.

——, W. Viezee, R. D. Hake, Jr., and R. T. H. Collis, 1976: Lidar observations of the stratospheric aerosol: California, October 1972 to March 1974. *Quart. J. Roy. Meteor. Soc.*, **102,** 675–695.

——, T. J. Swissler and M. P. McCormick, 1979: Methodology for error analysis and simulation of lidar aerosol measurements. *Appl. Opt.*, **18,** 3783–3797.

——, T. J. Swissler, M. P. McCormick, W. P. Chu, J. M. Livingston and T. J. Pepin, 1981a: Satellite and correlative measurements of the stratospheric aerosol I. An optical model for data conversions. *J. Atmos. Sci.*, **38,** 1279–1294.

——, M. P. McCormick, T. J. Swissler, M. P. Chu, J. M. Livingston, W. H. Fuller, J. M. Rosen, D. J. Hofmann, L. R. McMaster, D. C. Woods and T. J. Pepin, 1981b: Satellite and correlative measurements of the stratospheric aerosol II. Comparison of measurements made by SAM II, dustsondes, and an air-borne lidar. *J. Atmos. Sci.*, **38,** 1295–1312.

Steele, H. M., and P. Hamill, 1981: Effects of temperature and humidity on the growth and optical properties of sulphuric acid-water droplets in the stratosphere. *J. Aerosol Sci.*, **12,** 517–528.

Toon, O. B., and J. B. Pollack, 1973: Physical properties of the stratospheric aerosols. *J. Geophys. Res.*, **78,** 7051–7059.

——, and ——, 1976: A global average model of atmospheric aerosol for radiative transfer calculations. *J. Appl. Meteor.*, **15,** 225–246.

——, R. P. Turco, P. Hamill, C. S. Kiang and R. C. Whitten, 1979: A one-dimensional model describing aerosol formation and evolution in the stratosphere: II. Sensitivity studies and comparison with observations. *J. Atmos. Sci.*, **36,** 718–736.

Turco, R. P., P. Hamill, O. B. Toon, R. C. Whitten and C. S. Kiang, 1979: A one-dimensional model describing aerosol formation and evolution in the stratosphere: I. Physical processes and numerical analogs. *J. Atmos. Sci.*, **36,** 699–717.